Coupled-mode approach to the nonlinear dynamics induced by an elliptically polarized laser field in liquid crystals at normal incidence

A. Vella, B. Piccirillo, and E. Santamato
Istituto Nazionale di Fisica della Materia, Dipartimento di Scienze Fisiche, Università di Napoli "Federico II," via Cintia, 80126 Napoli, Italy

(Received 27 July 2001; published 12 February 2002)

A coupled-mode theory is presented to describe the dynamics of the molecular director induced by an elliptically polarized light plane wave normally incident onto a homeotropic liquid crystal film. The model provides a set of time ordinary differential equations for the lowest two modes of the system while the influence of the higher-order twist modes is accounted for by means of the adiabatic approximation. The resulting dynamics is complex above the reorientation threshold, according to the intensity and polarization of the incident light, rotating, oscillating, or steady states may settle. The dynamical regimes have been studied as functions of external parameters. The agreement with the experimental data was very good.

DOI: 10.1103/PhysRevE.65.031706 PACS number(s): 42.70.Df, 42.65.−k, 61.30.Gd

I. INTRODUCTION

The optical-field-induced molecular reorientation in liquid crystals (LCs) has been extensively studied in the last two decades and on this subject there are many reviews [1–4] and some chapters of general textbooks [5–7] that the reader can refer to. It was realized very soon, however, that the dynamics of the optical reorientation was much richer than the case of the magnetic-field-induced reorientation, because of the possible occurrence of self-induced stimulated light scattering [8] and angular momentum transfer from light to liquid crystals [9]. For instance, the optical Fréedericksz transition (OFT) induced by a linearly polarized laser beam normally incident onto a homeotropically aligned LC film was proved to be second order [10,11] (as the magnetic-field-induced Fréedericksz transition), but it becomes first order when circularly polarized light is used instead [9]. Also the dynamics of the OFT is dramatically changed. In the case of linear polarization of the incident beam, a monotonic approach to the final distorted state is observed [11], while for circular polarization a steady regime of uniform precession of the molecular director **n** around the beam axis is established [9]. In the case of elliptical polarization of the incident beam, a complex dynamics of **n** is induced, ranging from steady states to persistent oscillations and nonuniform precessions [12]. The main difference between the cases of linear and elliptical polarization is that in the first case the light polarization remains unchanged and the molecular distortion can be described by the polar angle θ of $\mathbf{n}=(\sin\theta\cos\phi,\sin\theta\sin\phi,\cos\theta)$ only, while in the second case both θ and ϕ angles come into play and the polarization state of the light changes with both space and time. It can be expected, therefore, that in the last case the dynamics may be very complex, as it is indeed observed. The basic equations governing the optically induced molecular reorientation as well as the light polarization state were deduced for normal incidence and arbitrary polarization of the incident beam in the plane-wave geometric optics approximation [13]. In the case of linear polarization, these equations reduce to the well-known equations governing the standard OFT [14] and in the case of circular polarization to the equations considered in Ref. [15]. A numerical brute force integration of the partial differential equations given in Ref. [13] showed that all dynamical regimes observed in the field of an elliptically polarized laser beam could be reproduced [12], but an analytical model has been lacking up to now.

In this paper we present a simple dynamical model able to describe the optical reorientation induced in a LC film by a laser beam at normal incidence with arbitrary polarization. Our model is based on the expansion of the polar angles $\theta(z,t)$ and $\phi(z,t)$ of **n** along suitable complete sets of normal modes. Inserting the mode expansions into the starting equations, a set of coupled time ordinary differential equations (ODEs) was derived. The higher-order modes have been adiabatically eliminated by the Galerkin method so as to obtain a set of only two ODEs for the coefficient $\theta_0(t)$ of the lowest-order mode in the θ expansion and the coefficient $\phi_0(t)$ of the lowest mode in the ϕ expansion. The two ODEs have been integrated numerically with respect to time and the resulting dynamics have been studied as a function of the incident light intensity and polarization. The agreement with the experimental data reported in Ref. [12] is remarkable: all the observed dynamical regimes have been reproduced in the right sequence with respect to the control parameters. It is worth noting that the first twist mode ϕ_1 was retained, although in its adiabatic approximation $\phi_1\cong\overline{\phi}_1(\theta_0,\phi_0)$, the complete suppression of ϕ_1, in fact, would rule out the nonlinear oscillations. Since $\overline{\phi}_1$ is related to the presence of twist in the sample, we conclude that some amount of twist must be present during oscillations.

II. THE TORQUE EQUATIONS

Let us consider a light plane wave normally incident onto a homeotropically aligned nematic film with thickness L. The anchoring forces at the walls located at $z=0$ and $z=L$ are assumed to be very strong. The polarization of the incident wave is arbitrary and its intensity (z component of the Poynting vector) is denoted as I. The torque equations for the polar angles $\theta(z,t)$ and $\phi(z,t)$ of the molecular director **n** are (cgs units are used)

$$\dot{\theta}=(1-p_1\sin^2\theta)\theta''-p_1\sin\theta\cos\theta\theta'^2-(1-2p_2\sin^2\theta)\times\sin\theta\cos\theta\phi'^2+(\tilde{I}/2n_0\mu)\overline{n_1}(\theta)(1+\Omega\cdot s),$$

$$\sin^2\theta\dot{\phi}=\partial/\partial u[(1-p_2\sin^2\theta)\sin^2\theta\phi']+(\tilde{I}/n_0\mu)[\overline{n}(\theta)-n_0](\mathbf{\Omega}\times\mathbf{s})_z, \quad (1)$$

where the dot means the partial derivative with respect to the reduced time $\tilde{t}=t/\tau$ with $\tau=\gamma_1 L^2/\pi^2 k_{33}$, the prime means the partial derivative with respect to the reduced coordinate $u=\pi z/L(u\in[0,\pi|)$ and the following quantities have been introduced:

$$\mu=1-\frac{n_0^2}{n_e^2}\quad(n_e>n_0),$$

$$p_1=1-\frac{k_{11}}{k_{33}},$$

$$p_2=1-\frac{k_{22}}{k_{33}},$$

$$\overline{n}(\theta)=\frac{n_0}{\sqrt{1-\mu\sin^2\theta}},$$

$$\overline{n_1}(\theta)=\frac{d\overline{n}}{d\theta},$$

$$I_{th}=\frac{c\pi^2 k_{33}}{n_0\mu L^2}, \quad (2)$$

and $\mathbf{\Omega}(u,t)=(\cos 2\phi,\sin 2\phi,0)$. In Eqs. (1) and (2) n_0 and n_e are the ordinary and extraordinary indexes of the liquid crystal and the k_{ii} $(i=1,2,3)$ are the elastic constants for splay, twist, and bend, respectively. For a typical liquid crystal material such as E7 at room temperature, $k_{11}=11.09\times10^{-7}$ dyne, $k_{22}=5.82\times10^{-7}$ dyne, $k_{33}=15.97\times10^{-7}$ dyne. For a sample with thickness $L\approx50$ μm, the characteristic time τ is typically $\tau=3$ s. The reduced Stokes vector $\mathbf{s}(u,t)=(s_1,s_2,s_3)$ is used to describe the light polarization inside the sample. The spatial evolution of $\mathbf{s}$ is governed by

$$\mathbf{s}'=(2L/\lambda)[\overline{n}(\theta)-n_0](\mathbf{\Omega}\times\mathbf{s}), \quad (3)$$

where λ is the optical wavelength in vacuum. The boundary conditions for Eqs. (1) and (3) are

$$\theta(0,t)=\theta(\pi,t)=0,$$

$$\phi'(0,t)=\phi'(\pi,t)=0,$$

$$\mathbf{s}(0,t)=\mathbf{s}_0=(s_{10},s_{20},s_{30}), \quad (4)$$

where $\mathbf{s}_0$ is the reduced Stokes vector of the polarization of the incident wave. Another useful quantity is the phase change $\alpha(t)$ suffered by the optical wave at time t in traversing the liquid crystal film,

$$\alpha(t)=\frac{2L}{\lambda}\int_0^\pi[\overline{n}(\theta(u,t))-n_0]du. \quad (5)$$

We notice that Eqs. (1)–(5) are invariant under the change

$$\phi\to\phi+\pi. \quad (6)$$

We assume a small splay-bend and a small twist distortion in the sample, so that $\theta(u,t)\ll1$ and $\phi'(u,t)\ll1$ (the angle ϕ itself may be large). Retaining terms up to the third order in θ and to the first order in ϕ', the torque Eqs. (1) reduce to

$$\dot{\theta}=(1-p_1\theta^2)\theta''-p_1\theta\theta'^2+\tilde{I}\left[\theta-\left(\frac{2}{3}-\frac{3\mu}{2}\right)\theta^3\right]\left(\frac{1+\mathbf{\Omega}\cdot\mathbf{s}}{2}\right), \quad (7)$$

$$\dot{\phi}=\frac{1}{\theta^2}\frac{\partial}{\partial u}\left(\theta^2\frac{\partial\phi}{\partial u}\right)+(\tilde{I}/2)(\mathbf{\Omega}\times\mathbf{s})_z. \quad (8)$$

In the same approximation, Eqs. (3) and (5) yield

$$\mathbf{s}'=\left(\frac{\mu n_0 L}{\lambda}\right)\theta^2(\mathbf{\Omega}\times\mathbf{s}), \quad (9)$$

$$\alpha(t)=\left(\frac{\mu n_0 L}{\lambda}\right)\int_0^\pi\theta^2(u,t)du. \quad (10)$$

III. THE MODE EXPANSION

We expand the fields $\theta(u,t)$ and $\phi(u,t)$ in terms of complete sets of orthogonal functions

$$\theta(u,t)=\sum_{n=0}^{\infty}\theta_n(t)V_n(u), \quad (11)$$

$$\phi(u,t)=\sum_{n=0}^{\infty}\phi_n(t)U_n(\cos u)=\phi_0(t)+\phi_d(u,t), \quad (12)$$

where $U_n(\cos u)=\sin[(n+1)u]/\sin u$ are the Chebyshev polynomials of the second kind [16] and $V_n(u)$ are given by $V_n(u)=U_n(\cos u)\sin u=\sin[(n+1)u]$. These functions are normalized according to

$$\int_0^\pi V_m(u)V_n(u)du=\int_0^\pi U_m(\cos u)U_n(\cos u)\sin^2 u\,du=\frac{\pi}{2}\delta_{nm}. \quad (13)$$

The angles $\theta(u,t)$ and $\phi(u,t)$ defined in Eqs. (11) and (12) obey the boundary conditions given by Eqs. (4). In Eq. (12) we split out the term $\phi_d(u,t)=\Sigma_{n=1}^{\infty}\phi_n(t)U_n(\cos u)$, describing the twist distortion of the molecular director, from the zero-order term $\phi_0(t)$. The term $\phi_0(t)$ corresponds, in fact, to a rigid rotation of $\mathbf{n}$ and does not involve an elastic distortion in the sample. We assumed, as said before, a very small elastic distortion. Then, we may retain only the lowest-order mode in Eq. (11),

$$\theta(u,t) \simeq \theta_0(t)\sin u, \tag{14}$$

and assume $\theta_0(t)$ and $\phi_d(u,t)$ to be very small quantities. We notice, however, that $\phi_0(t)$ is allowed to be large at will. Inserting Eq. (11) into Eq. (7) and projecting the resulting equation along the zero-order mode $V_0(u)$ yields a single equation for $\theta_0(t)$,

$$\dot{\theta}_0 = -\theta_0 + \frac{p_1}{2}\theta_0^3 + (\tilde{I}/2)\left[\theta_0 - \left(\frac{4-9\mu}{8}\right)\theta_0^3\right] + (\tilde{I}/\pi)\theta_0 \int_0^\pi [(\mathbf{\Omega}_0 + \mathbf{\Omega}_1)\cdot \mathbf{s}]\sin^2 u\, du - (\tilde{I}/\pi)\left(\frac{2}{3} - \frac{3\mu}{2}\right)\theta_0^3 \int_0^\pi (\mathbf{\Omega}_0 \cdot \mathbf{s})\sin^4 u\, du, \tag{15}$$

where we expand $\mathbf{\Omega}(u,t)$ according to

$$\mathbf{\Omega} = \mathbf{\Omega}_0(t) + \mathbf{\Omega}_1(u,t) \tag{16}$$

with $\mathbf{\Omega}_0(t) = (\cos 2\phi_0(t), \sin 2\phi_0(t), 0)$ and $\mathbf{\Omega}_1(u,t) = 2\phi_d(u,t)(-\sin 2\phi_0(t), \cos 2\phi_0(t), 0)$. Since $\phi_d(u,t)$ is small, we neglected the term containing $\mathbf{\Omega}_1(u,t)$ in the last term on the right of Eq. (15), containing the already small quantity θ_0^3. In the same approximation, the optical phase change $\alpha(t)$ reduces to

$$\alpha(t) = \tilde{L}\,\theta_0^2(t), \tag{17}$$

where $\tilde{L} = (\pi\mu n_0/2\lambda)L$. Inserting Eq. (17) into Eq. (15) we get the following differential equation for the optical phase change $\alpha(t)$:

$$\dot{\alpha} = (\tilde{I}-2)\alpha + \left[\tilde{I}\left(\frac{9\mu-4}{8}\right) + p_1\right]\frac{\alpha^2}{\tilde{L}} + \tilde{I}\alpha\left(\frac{2}{\pi}\right) \times \int_0^\pi [(\mathbf{\Omega}_0 + \mathbf{\Omega}_1)\cdot \mathbf{s}]\sin^2 u\, du - \tilde{I}\left(\frac{2}{3} - \frac{3\mu}{2}\right)\frac{\alpha^2}{\tilde{L}}\left(\frac{2}{\pi}\right) \times \int_0^\pi (\mathbf{\Omega}_0 \cdot \mathbf{s})\sin^4 u\, du. \tag{18}$$

Inserting Eq. (14) into Eq. (8) yields

$$\dot{\phi} = \frac{1}{\sin^2 u}\frac{\partial}{\partial u}(\sin^2 u\,\phi') + (\tilde{I}/2)(\mathbf{\Omega}\times\mathbf{s})_z. \tag{19}$$

Projecting this equation along the modes U_n yields

$$\dot{\phi}_n = -n(n+2)\phi_n + (\tilde{I}/\pi)\int_0^\pi [(\mathbf{\Omega}_0 + \mathbf{\Omega}_1)\times\mathbf{s}]_z \times U_n(\cos z)\sin^2 u\, du \quad (n = 0,1,\ldots). \tag{20}$$

Equations (15) and (20) are coupled by means of the Stokes vector **s**. We must therefore solve the light polarization problem first.

IV. THE LIGHT POLARIZATION PROBLEM

In the small distortion approximation, Eq. (9) becomes

$$\mathbf{s}' = (2\alpha/\pi)\sin^2 u[(\mathbf{\Omega}_0 + \mathbf{\Omega}_1)\times\mathbf{s}], \tag{21}$$

where α is given by Eq. (17). These equations can be solved perturbatively using $\phi_d(u,t)$ as a small parameter. At the first significant order, the solution is

$$\begin{aligned} s_1 &= s_{10} + \sin 2\phi_0[(s_{20}\cos 2\phi_0 - s_{10}\sin 2\phi_0)(1-\cos\alpha v) + s_{30}\sin\alpha v] + \epsilon\cos 2\phi_0, \\ s_2 &= s_{20} - \cos 2\phi_0[(s_{20}\cos 2\phi_0 - s_{10}\sin 2\phi_0)(1-\cos\alpha v) + s_{30}\sin\alpha v] + \epsilon\sin 2\phi_0, \\ s_3 &= s_{30} + (s_{20}\cos 2\phi_0 - s_{10}\sin 2\phi_0)\sin\alpha v - s_{30}(1-\cos\alpha v), \end{aligned} \tag{22}$$

where

$$v(u) = \frac{u - \sin u\cos u}{\pi} \quad (v \in [0,1]) \tag{23}$$

and

$$\epsilon = 2\alpha\int_0^v [s_{30}\cos\alpha w + (s_{20}\cos 2\phi_0 - s_{10}\sin 2\phi_0)\sin\alpha w]\phi_d(w,t)\,dw \tag{24}$$

is a small quantity proportional to the twist distortion ϕ_d. Without loss of generality, we may choose the x axis along the major axis of the polarization ellipse of the incoming light, so that $s_{10} = \cos 2\chi$, $s_{20} = 0$, $s_{30} = \sin 2\chi$ with angle $\chi \in [0, \pi/4]$.

V. THE COUPLED-MODE EQUATIONS

Inserting Eq. (22) into Eqs. (18) and (20) we obtain

$$\begin{aligned} \dot{\alpha} &= [\tilde{I}(1 + \cos 2\chi\cos 2\phi_0 + F_1) - 2]\alpha + \left[\tilde{I}\left(\frac{9\mu-4}{8}\right)(1+\cos 2\chi\cos 2\phi_0) + p_1\right]\frac{\alpha^2}{\tilde{L}}, \\ \dot{\phi}_0 &= -(\tilde{I}/2\alpha)[\sin 2\chi(1-\cos\alpha) + \cos 2\chi\sin 2\phi_0\sin\alpha], \\ \dot{\phi}_n &= -n(n+2)(\phi_n - \overline{\phi_n}) \quad (n = 1,2,\ldots), \end{aligned} \tag{25}$$

where $\overline{\phi_n}$ are given by

$$\overline{\phi_n} = -\frac{\tilde{I}}{2n(n+2)}\sin 2\chi A_n(\alpha) + \cos 2\chi\sin 2\phi_0 B_n(\alpha)] \quad (n = 1,2,\ldots) \tag{26}$$

and F_1 is given by

$$F_1 = \sum_{n=1}^{\infty} f_n \phi_n ,$$

$$f_n = -2 \sin 2\chi [A_n(\alpha) - C_n(\alpha)] + \cos 2\chi \times \sin 2\phi_0 [B_n(\alpha) + D_n(\alpha)]. \quad (27)$$

In Eqs. (26) and (27), we introduced the functions

$$A_n(\alpha) = \int_0^1 \sin \alpha v U_n(\cos u(v)) dv ,$$

$$B_n(\alpha) = \int_0^1 \cos \alpha v U_n(\cos u(v)) dv ,$$

$$C_n(\alpha) = \alpha \int_0^1 (1-u) \cos \alpha u U_n(\cos z(u)) du ,$$

$$D_n(\alpha) = \alpha \int_0^1 (1-u) \sin \alpha u U_n(\cos z(u)) du . \quad (28)$$

Equations (25) form an infinite set of coupled ODEs for $\alpha(t)$, $\phi_0(t)$, and $\phi_n(t)$ $(n=1,2,\ldots)$. As shown in the last of Eqs. (25), the modes ϕ_n are highly damped, with damping constants increasing with n as $n(n+2)$. We may assume, therefore, that the modes ϕ_n follow adiabatically their steady state values $\overline{\phi_n}$ given by Eq. (26). When the modes ϕ_n are adiabatically eliminated, by setting $\phi_n = \overline{\phi_n}$ (Galerkin method), we are left with the first two of Eqs. (25) only and the degrees of freedom of our system reduce to α and ϕ_0. Moreover, Eq. (26) shows that the values $\overline{\phi_n}$ are rapidly decreasing functions of n, so that we may retain only a few of them. If all the twist modes were neglected setting $\phi_n = 0$, the first two of Eqs. (25) would reduce to the set of equations already studied in Ref. [17]. In this approximation, however, there is no way to obtain the oscillations of the director **n**, which instead have been observed experimentally [12]. We conclude that *the twist degrees of freedom are essential to induce the nonlinear oscillations*. Moreover, just adding the first torsional mode ϕ_1, even in its adiabatic approximation $\phi_1 = \overline{\phi_1}$, is enough to produce the oscillating regime. Adding further adiabatic modes $\overline{\phi_n}$ (we tried up to $n=64$ modes) produces no appreciable change in the dynamics. Similarly, releasing the adiabatic approximation for the dominant twist mode setting $\phi_1 = \phi_1(t)$ adds no new feature. Then, in order to have a model as simple as possible, we take only the first two of Eqs. (25) with F_1 given by $F_1 = f_1 \overline{\phi_1}$. The results obtained in this way and their connection with the experimental data will be discussed in the following sections. Here we notice that the integrals defining the functions $A_n(\alpha), B_n(\alpha), C_n(\alpha), D_n(\alpha)$ can be evaluated dynamically at each step of the numerical integration of our two ODEs exploiting the numerical fast Fourier transform algorithm, with no appreciable increase of the total integration time.

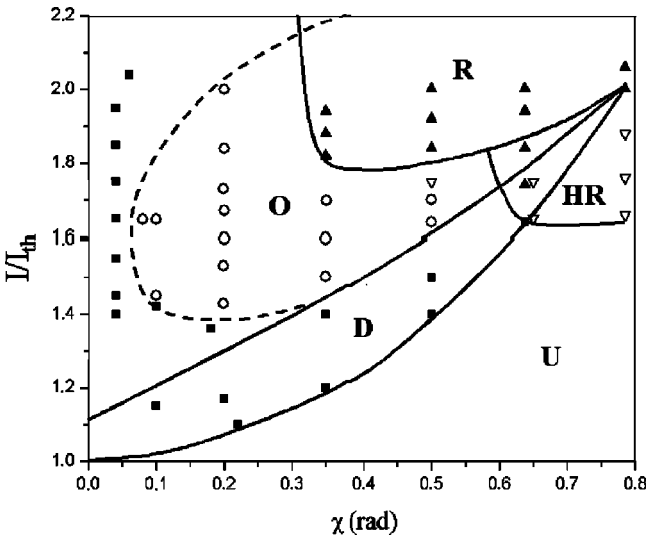

FIG. 1. Map of the dynamical regimes in the $(\tilde{I},\chi)$ plane. The points refer to the experimental observations [12]. Undistorted states (U); ■ distorted states (D); ○ oscillating states (O); ▲ rotating states (R); ▽ hysterical rotating states (HR).

VI. THE MAP OF THE REGIMES

In Fig. 1 we present a map of the dynamical regimes in the parameter plane $(\tilde{I},\chi)$. The points are the experimental data taken from Ref. [12]. The different dynamical regimes are separated by critical curves. We can locate three regions of ellipticity with different dynamical behavior: almost linear polarization $(0 \leqslant \chi \lesssim \pi/10)$, only distorted and oscillating states are present; intermediate ellipticity $(\pi/10 \lesssim \chi \lesssim \pi/6)$, distorted, oscillating, and rotating states are present; almost circular polarization $(\pi/6 \lesssim \chi \lesssim \pi/4)$, hysteresis between oscillating and rotating regimes is present. As shown in Fig. 1 the agreement between theory and experiment is very good, in spite of the fact that only two ODEs were used. Some considerations are in order, however. First, the data have been corrected for thermal heating of the sample, as indicated in Ref. [12]. Heating in fact produces a lowering of the liquid crystal order parameter and hence a lowering of the elastic constants with increasing optical power. Second, when we changed the intensity $\tilde{I}$ (for fixed ellipticity angle χ), we take as initial data to integrate the differential equations the final data of the previous run. This procedure simulates an abrupt increase of the incident laser intensity, so that the system has no time to move. This yields the solid critical curves drawn in Fig. 1. If, instead, we simulate a very little relaxation of the system by slightly changing the initial conditions during the change of $\tilde{I}$ (only one part of 10^{-4} is enough), the critical line separating the steady states from the oscillations is changed into the dotted one. The difference between the two cases is particularly evident in the almost linear polarization region: the presence of a small relaxation quenches the transition to the oscillation regime and the distorted steady state remains stable, as observed in the experiments. This behavior may be explained considering that the attraction basin of the limit cycle corresponding to oscillations becomes negligibly small as the light polarization tends

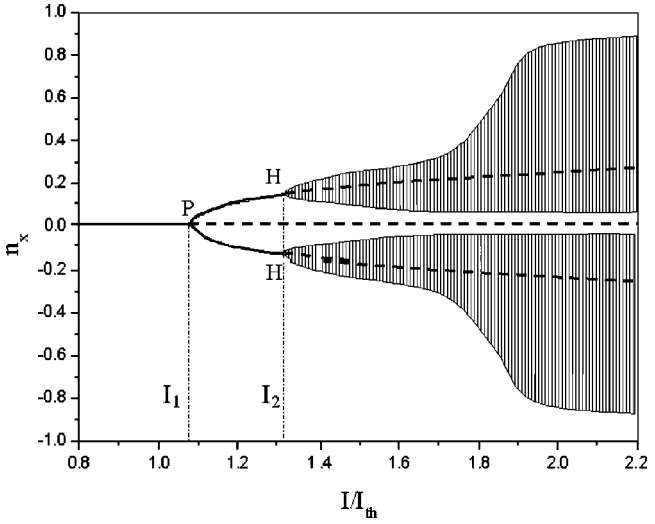

FIG. 2. The solution diagram for $\chi=\pi/12$ (solid line, stable stationary solutions; dashed lines, unstable stationary solutions). The dashed regions represent the amplitude of the *x* projection of the oscillating cycles. The two symmetrical regions remain always separated.

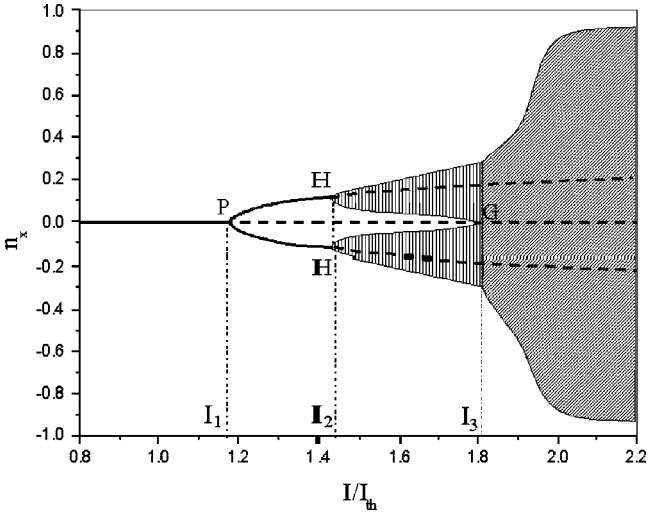

FIG. 3. The solution diagram for $\chi=\pi/8$ (solid line, stationary solutions; dashed lines, unstable stationary solutions). The vertically dashed regions represent the amplitude of the *x* projection of the oscillating cycles that over the gluing point I_3 merge into rotating cycles, represented by the obliquely dashed regions.

to be linear. So very particular initial data are needed to drive the system into its oscillation state. Because of the presence of relaxation and of unavoidable noise, during the intensity change, the oscillation regimes are not reached in practice with almost linearly polarized light.

VII. BIFURCATION ANALYSIS

Solution diagrams in the three different regions of the parameter χ were obtained with a continuation algorithm. Figure 2 shows the stationary and periodic solutions for $\chi=\pi/12$ (first region). For the sake of illustration, the director component $n_x=\sin\theta_0\cos(\phi_0-2\phi_1)$, with θ_0 derived from Eq. (17), is reported versus the normalized intensity $\tilde{I}$ of the optical wave. When $\tilde{I}$ is below the threshold value $\tilde{I}=I_1=2/(1+\cos 2\chi)$ for the OFT, the only stable state is the undistorted one $n_x=n_y=0$. At the threshold value I_1 a pitchfork bifurcation is encountered (P). Above the threshold, the undistorted state becomes unstable and a new stable distorted state appears. Because of the symmetry of the system, a second branch is obtained from the first under the change (6) for a fixed value of $\tilde{I}$. Going on increasing the intensity $\tilde{I}$, the distorted state remains stable, until the second critical value I_2 is reached where a Hopf bifurcation (H) occurs and the system evolves towards a limit cycle corresponding to nonlinear oscillations of **n**. The boundaries of the dashed regions yield, for fixed $\tilde{I}$, the maximum and minimum value that n_x reaches during the cycle.

The solution diagram for $\chi=\pi/8$ (second region) is reported in Fig. 3. This diagram shows the same behavior and bifurcations as the previous one for $\tilde{I}<I_3$. For this intensity value a gluing bifurcation is found (G), where the cycle is gluing with the symmetric one obtained under the transformation (6). After the two cycles have been glued together, the director motion develops along a large limit cycle enclosing the origin, which corresponds to the rotation of **n**. An example of trajectories in the (n_x,n_y) plane is shown in Fig. 4 for different intensity values near the gluing point. The transition point (G) between the oscillation and rotation is a homoclinic bifurcation, where the motion suffers a marked slowing down in time. This is shown in Fig. 5 where the period of the motion is plotted as a function of $\tilde{I}$: a search for a critical slowing down exponent yielded $T/\tau\propto(\tilde{I}-I_3)^{-\gamma}$ with $\gamma=0.118\pm0.005$. The exponent γ was found to be the same on both sides of the critical point I_3. Unfortunately, we found no measurements on the slowing down effect in the literature. For $\tilde{I}>\tilde{I}_3$, the rotation cycle remains stable.

For $\chi=0.6$ (third region) the solution diagram shows a further branch of periodic solutions for $I_5<\tilde{I}<I_4$ as shown

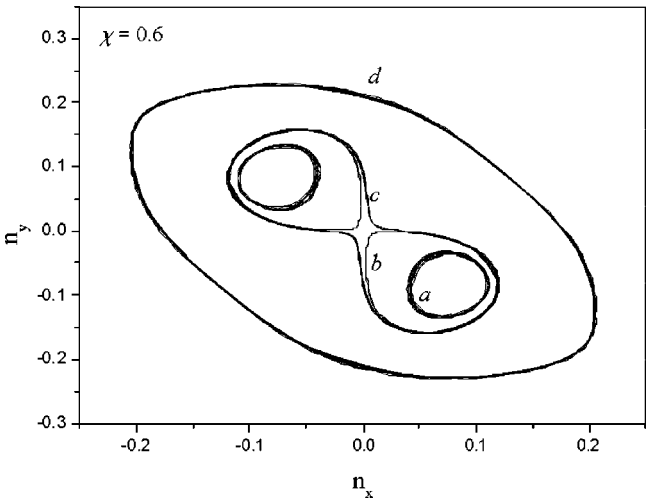

FIG. 4. The trajectories in the phase space for $\chi=0.6$. The cycles correspond to the following intensity values: (a) $\tilde{I}=1.808$, (b) $\tilde{I}=1.828$, (c) $\tilde{I}=1.832$, and (d) $\tilde{I}=1.920$.

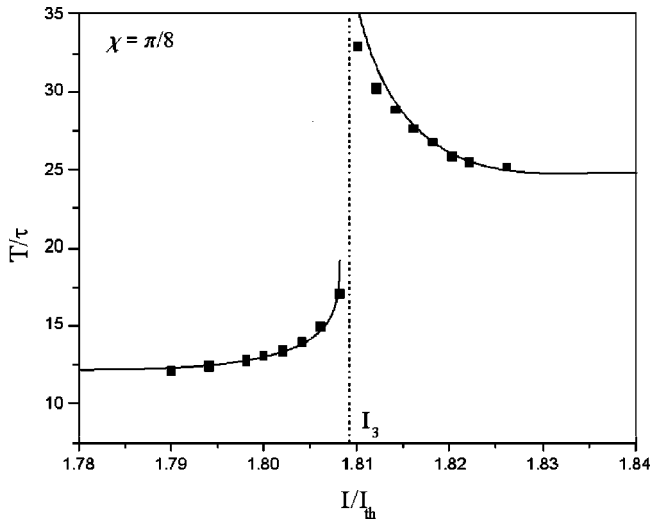

FIG. 5. The period T of the motion near the transition point I_3 as a function of $\tilde{I}$. The solid line is the best fit for the scaling law $T/\tau \propto (\tilde{I}-I_3)^{-\gamma}$ with $\gamma = 0.118 \pm 0.005$.

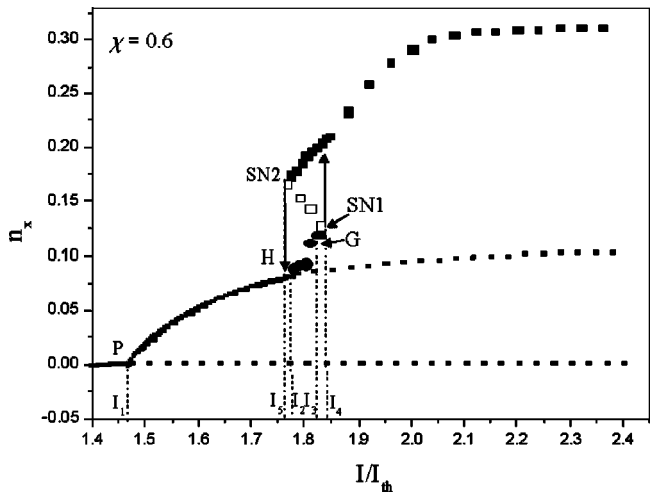

FIG. 6. The solution diagram for $\chi = 0.6$ showing the hysteresis of the rotation regime. Branch *PH* (solid line): stationary distorted states. Branch *HG* (filled circles): peak value of n_x in the oscillating states; the oscillation center is on the dashed line starting form *H*. Upper branch (filled squares): peak value of n_x in the rotating states; the center of rotation is the dashed line at $n_x = 0$. The states indicated by empty squares are unstable. The vertical arrows mark transitions between different regimes.

in Fig. 6. This branch corresponds to a hysteretical regime as experimentally observed. Increasing $\tilde{I}$ above the gluing value I_3 a new bifurcation point (saddle-node, SN1) is encountered at $I = \tilde{I}_4$, where the system jumps to cycles with larger and larger diameters. For the intensity values $I_5 < \tilde{I} < I_4$ three branches of periodical regimes are possible, two stable and one unstable. The transition point (SN2) at $\tilde{I} = I_5$ corresponds to a point of saddle-node bifurcation where the unstable branch disappears. When $\tilde{I}$ is decreased down to SN2, the system jumps to either a distorted steady state (as in the case shown in Fig. 6) or directly to the undistorted state, depending on the value of χ.

VIII. CONCLUSIONS

We presented a coupled-mode approach to the optical reorientation induced in a liquid crystal film by a light plane wave at normal incidence. Depending on the light polarization and intensity, different dynamical regimes of the molecular director are induced: rotations, oscillations, and distorted steady states. In spite of the simplicity of the model (only two ODEs), all experimental findings are well reproduced, including the hysteresis between rotations and oscillations at large ellipticity χ. The transition from the distorted steady states to the oscillation regime was found to be a Hopf bifurcation, while the transition from oscillations to rotations turned out to be associated to the gluing of two limit cycles through the homoclinic bifurcation point. An interesting aspect of our model is that the addition of small noise to the initial conditions, when the intensity is changed, tends to maintain the system in a distorted steady state, avoiding the occurrence of nonlinear oscillations. This behavior is particularly evident when the light polarization is almost linear and it explains why the multistability foreseen in the case of a linearly polarized light beam [17] has never been observed in practice.

ACKNOWLEDGMENT

We thank INFM (Istituto Nazionale per la Fisica della Materia) for financial support.

[1] N. V. Tabiryan, A. V. Sukhov, and B. Y. Zel'dovich, Mol. Cryst. Liq. Cryst. **136**, 1 (1986).
[2] I. C. Khoo, Prog. Opt. **26**, 107 (1988).
[3] E. Santamato, in *Nonlinear Optical Material and Devices for Applications in Information Technology*, edited by A. Miller *et al.* (Kluwer Academic, Dordrecht, 1995), pp. 103–139.
[4] E. Santamato and Y. R. Shen, in *A Guide to Liquid Crystal Research*, edited by P. J. Collings and J. S. Patel (Oxford University Press, New York, 1997), Chap. 14, pp. 539–566.
[5] I. C. Khoo and S. T. Wu, *Optics and Nonlinear Optics of Liquid Crystals* (World Scientific, Singapore, 1993), Vol. 1.
[6] I. C. Khoo and F. Simoni, *The Physics of Liquid Crystalline Materials* (Gordon and Breach, New York, 1991).
[7] F. Simoni, *Nonlinear Optical Properties of Liquid Crystals and PDLC*, Series on Liquid Crystals Vol. 2 (World Scientific, Singapore, 1997).
[8] E. Santamato, B. Daino, M. Romagnoli, M. Settembre, and Y. R. Shen, Phys. Rev. Lett. **61**, 113 (1988).
[9] E. Santamato, B. Daino, M. Romagnoli, M. Settembre, and Y. R. Shen, Phys. Rev. Lett. **57**, 2423 (1986).
[10] A. S. Zolot'ko, V. F. Kitaeva, N. Kroo, N. I. Sobolev, and L. Csillag, Sov. Phys. JETP **32**, 158 (1980).

[11] S. D. Durbin, S. M. Arakelian, and Y. R. Shen, Phys. Rev. Lett. **47**, 1411 (1981).
[12] E. Santamato, G. Abbate, P. Maddalena, L. Marrucci, and Y. R. Shen, Phys. Rev. Lett. **64**, 1377 (1990).
[13] E. Santamato, G. Abbate, and P. Maddalena, Phys. Rev. A **38**, 4323 (1988).
[14] H. L. Ong, Phys. Rev. A **28**, 2393 (1983).
[15] L. Marrucci, G. Abbate, S. Ferraiuolo, P. Maddalena, and E. Santamato, Phys. Rev. A **46**, 4859 (1992).
[16] *Handbook of Mathematical Functions*, edited by M. Abramowitz and I. A. Stegun (Dover, New York, 1970).
[17] G. Abbate, P. Maddalena, L. Marrucci, L. Saetta, and E. Santamato, J. Phys. II **1**, 543 (1991).